Nitric oxide-induced calcium release via ryanodine receptors regulates neuronal function

Sho Kakizawa[1,2,3,8,*], Toshiko Yamazawa[1,8], Yili Chen[4], Akihiro Ito[4], Takashi Murayama[5], Hideto Oyamada[6], Nagomi Kurebayashi[5], Osamu Sato[5], Masahiko Watanabe[7], Nozomu Mori[2], Katsuji Oguchi[6], Takashi Sakurai[5], Hiroshi Takeshima[3], Nobuhito Saito[4], and Masamitsu Iino[1,*]

[1]Department of Pharmacology, Graduate School of Medicine, The University of Tokyo, Tokyo 113-0033, Japan.
[2]Department of Anatomy and Neurobiology, Graduate School of Biomedical Sciences, Nagasaki University, Nagasaki 852-8523, Japan.
[3]Department of Biological Chemistry, Kyoto University Graduate School of Pharmaceutical Sciences, Kyoto 606-8501, Japan.
[4]Department of Neurosurgery, Graduate School of Medicine, The University of Tokyo, Tokyo 113-0033, Japan.
[5]Department of Pharmacology, Juntendo University School of Medicine, Tokyo 113-8421, Japan.
[6]Department of Pharmacology, School of Medicine, Showa University, Tokyo 142-8555, Japan.
[7]Department of Anatomy, Hokkaido University School of Medicine, Sapporo 060-8638, Japan.
[8]These authors contributed equally to this work.

*Corresponding authors. M Iino, Department of Pharmacology, Graduate School of Medicine, The University of Tokyo, Tokyo 113-0033, Japan. Tel.: +81 3 5841 3417; Fax: +81 3 5841 3390; E-mail: iino@m.u-tokyo.ac.jp or S Kakizawa, Department of Biological Chemistry, Kyoto University Graduate School of Pharmaceutical Sciences, Kyoto 606-8501, Japan; E-mail: sho-kaki@pharm.kyoto-u.ac.jp

Running title: Nitric oxide-induced Ca^{2+} release in the brain

Abstract

Mobilization of intracellular Ca^{2+} stores regulates a multitude of cellular functions, but the role of intracellular Ca^{2+} release via the ryanodine receptor (RyR) in the brain remains incompletely understood. We found that nitric oxide (NO) directly activates RyRs, which induce Ca^{2+} release from intracellular stores of central neurons, and thereby promote prolonged Ca^{2+} signaling in the brain. Reversible *S*-nitrosylation of type 1 RyR (RyR1) triggers this Ca^{2+} release. NO-induced Ca^{2+} release (NICR) is evoked by type 1 NO synthase-dependent NO production during neural firing, and is essential for cerebellar synaptic plasticity. NO production has also been implicated in pathological conditions including ischemic brain injury, and our results suggest that NICR is involved in NO-induced neuronal cell death. These findings suggest that NICR via RyR1 plays a regulatory role in the physiological and pathophysiological functions of the brain.

Keywords: Calcium / Nitric oxide / Ryanodine receptor / Synapse

Introduction

Intracellular Ca^{2+} signaling regulates a myriad of cellular functions (Berridge et al, 2000). In addition to Ca^{2+} influx from extracellular spaces, Ca^{2+} is mobilized within the cell from intracellular Ca^{2+} stores through two types of Ca^{2+} release channels: ryanodine receptors (RyRs) and inositol 1,4,5-trisphosphate receptors (IP_3Rs). The opening of RyRs is regulated by Ca^{2+} channels in the plasma membrane. Whereas the opening of type 2 RyR (RyR2) is regulated by an influx of Ca^{2+} via voltage-gated Ca^{2+} channels through the Ca^{2+}-induced Ca^{2+} release (CICR) mechanism in cardiac cells, type 1 RyR (RyR1) is physiologically regulated by voltage-gated Ca^{2+} channels through direct protein–protein interactions in skeletal muscle cells (Endo, 2009). Although RyR1 is also expressed in the brain, such tight Ca^{2+} channel-mediated regulation of intracellular Ca^{2+} release via RyR1, as seen in skeletal muscle cells, is absent in central neurons (Kano et al, 1995). Therefore, further investigation into the regulatory mechanisms and functions of RyR1 in the brain is warranted.

Nitric oxide (NO) is a ubiquitous intercellular gaseous messenger that is enzymatically generated by NO synthase (NOS) (Bredt & Snyder, 1994). In the brain, NO signaling regulates many physiological and pathophysiological functions, including synaptic plasticity and neuronal cell death. However, the mechanisms by which NO signaling regulates neuronal function require further clarification. *In vitro* single channel measurements suggest that NO enhances the probability of RyR1 channel opening through *S*-nitrosylation (Aghdasi et al, 1997; Eu et al, 2000). This mechanism is implicated in Ca^{2+} leak from skeletal muscle Ca^{2+} stores in pathological conditions (Bellinger et al, 2009;

Durham et al, 2008). However, the functional role of NO-dependent effects on RyR1 in the brain has not yet been elucidated.

Therefore, the objective of the present study was to assess if NO has an effect on RyR1-mediated Ca^{2+} signaling in central neurons. Our findings suggest that NO functions as a RyR1 agonist to release Ca^{2+} from neuronal intracellular Ca^{2+} stores through a reversible *S*-nitrosylation of the RyR1. The resulting Ca^{2+} signal is required for the induction of NO-dependent synaptic plasticity in the cerebellar synapses. NO generation is associated with many diseases of the brain. Our results suggest that NO-induced Ca^{2+} release via RyR1 is involved in neuronal cell death. These findings show a novel form of Ca^{2+} signaling in the brain that plays an important part in health and disease.

Results

NO induces Ca^{2+} release from neuronal intracellular Ca^{2+} stores

We examined potential functional interactions between NO and Ca^{2+} signaling in the cerebellar cortex, where NOS1 is highly expressed in granule cells (Bredt et al, 1991). The granule cells extend axons to form glutamatergic synapses on the dendrites of Purkinje cells (PCs), which abundantly express RyR1 (Furuichi et al, 1994). To our surprise, when an NO donor – NOC7 (1-Hydroxy-2-oxo-3-(*N*-methyl-3-aminopropyl)-3-methyl-1-triazene) or NOR1 ((±)-(*E*)-4-Methyl-2-[(*E*)-hydroxyimino]-5-nitro-6-methoxy-3-hexenamide) – was applied to acute cerebellar slices, the intracellular Ca^{2+} concentration ($[Ca^{2+}]_i$) increased in PC dendrites (Figure 1A and B; Supplementary Figure S1A). The NO-induced Ca^{2+} increase was observed in the absence of extracellular Ca^{2+} (Figure 1D; Supplementary Figure S1B), and was blocked using an inhibitor of the sarco(endo)plasmic reticulum Ca^{2+} ATPase, thapsigargin, which depletes Ca^{2+} stores (Figure 1B and D). These results suggest that NO mediates the release of Ca^{2+} from neuronal intracellular Ca^{2+} stores.

PCs express two types of Ca^{2+} release channels: RyR and IP_3R (Furuichi et al, 1994). Of all Ca^{2+} release channel subtypes, RyR1 and IP_3R1 are the most dominant subtypes expressed in PCs (Furuichi et al, 1994; Giannini et al, 1995; Mori et al, 2000; Sawada et al, 2008; Wojcikiewicz, 1995). We examined which of these two channels was responsible for the NO-induced $[Ca^{2+}]_i$ increase. Application of the IP_3R inhibitor heparin at a concentration (4 mg ml^{-1}) sufficient to inhibit IP_3R in PCs (Takechi et al, 1998) had no effect on the $[Ca^{2+}]_i$ increase (Figure 1D; Supplementary Figure S1C). Conversely, a RyR

inhibitor, dantrolene, blocked the NO-induced $[Ca^{2+}]_i$ increase at 36°C (the temperature at which the drug's effects are observed) (Zhao et al, 2001) (Figure 1C and D). Thus, RyR1, but not IP_3R, seems to be responsible for the NO-induced $[Ca^{2+}]_i$ increase. This notion was further examined in mice deficient in RyR1 (Takeshima et al, 1994). Because *Ryr1*$^{-/-}$ mice die perinatally, PCs in acute neonatal cerebellar slices were studied. Even though neonatal PCs have poor dendritic arborization, intracellular Ca^{2+} stores in the somata of *Ryr1*$^{+/+}$ PCs responded to NO to release Ca^{2+}, and this effect was blocked by thapsigargin and dantrolene (Figure 1E–G; Supplementary Figure S1D). However, NO did not induce Ca^{2+} increase in *Ryr1*$^{-/-}$ PCs (Figure 1E–G). The absence of NO-induced Ca^{2+} responses in *Ryr1*$^{-/-}$ PCs was not due to an impairment of Ca^{2+} stores, because glutamate-induced Ca^{2+} release was observed in the PCs of the mutant mice (Supplementary Figure S1E). These findings indicate that RyR1 underlies the NO-induced $[Ca^{2+}]_i$ increase.

NO-induced Ca^{2+} release in cells expressing exogenous RyR

We then characterized the agonistic effect of NO on RyR1 using HEK293 cells with tetracycline-regulated RyR1 expression (Supplementary Figure S2A and B). In control cells without exogenous RyR1 expression, neither NOC7 nor the RyR agonist, caffeine, induced a change in $[Ca^{2+}]_i$ (Supplementary Figure S2C). Conversely, RyR1-expressing cells demonstrated a clear Ca^{2+} response to both NOC7 (Figure 2A and C) and caffeine (Figure 2D) in a dose-dependent manner. This NO-induced Ca^{2+} increase was a reversible process (Supplementary Figure S2D), and this effect was completely blocked by thapsigargin or

dantrolene (Figure 2A; Supplementary Figure S2E and F). Taken together, these findings indicate that RyR1 activation is both necessary and sufficient for NO-induced Ca^{2+} release from intracellular stores. This mechanism will be hereafter referred to as 'NO-induced Ca^{2+} release' (NICR).

There are three subtypes of RyR, all of which are expressed in the brain. We examined if subtypes other than RyR1 also function via the NICR mechanism. Cells expressing RyR2 or RyR3 demonstrated a robust response to caffeine (Supplementary Figure S2G). RyR2 has high CICR activity, and cells expressing this subtype generated spontaneous Ca^{2+} oscillations (Supplementary Figure S2G). Despite this, the effect of NO on RyR2 Ca^{2+} release was very slight (Figure 2B; Supplementary Figure S2G). In contrast, cells expressing RyR3 responded to NO, although the sensitivity to NO appeared to be lower than that of RyR1 (Figure 2B; Supplementary Figure S2G). Thus, NICR occurs predominantly via RyR1, to a lesser extent via RyR3, and not via RyR2.

Underlying mechanisms of NO-induced Ca^{2+} release

NO exerts its effects via two pathways: activation of soluble guanylyl cyclase (sGC) and subsequent cyclic GMP (cGMP) signaling, as well as protein *S*-nitrosylation (Hess et al, 2005). It seems unlikely that NICR occurs via the sGC pathway, as its inhibitor 1*H*-[1,2,4]oxadiazolo[4,3-*a*]quinoxalin-1-one (ODQ) had no inhibitory effects on NICR (Figure 2A; Supplementary Figure S2E). We therefore examined the *S*-nitrosylation mechanism. RyR1 has several cysteine residues that are susceptible to *S*-nitrosylation, and

S-nitrosylation particularly at cysteine 3635 enhances the open probability of single RyR1 channels in planer bilayers (Moore et al, 1999; Sun et al, 2001). To examine the role of *S*-nitrosylation in NICR, we generated HEK293 cells expressing a mutated C3635A-RyR1, where the critical cysteine residue was replaced by alanine (Supplementary Figure S2B). Caffeine, but not NOC7, led to Ca^{2+} release in cells expressing C3635A-RyR1 (Figure 2C and D). Using the biotin-switch method, we then analyzed *S*-nitrosylation of RyR1 (Figure S2A). RyR1 was transiently *S*-nitrosylated by NOC7, but *S*-nitrosylation was significantly reduced in C3635A-RyR1 (Figure 2E and F). These results indicate that *S*-nitrosylation of RyR1 is the underlying mechanism of NICR. We also examined whether cerebellar RyR1 is *S*-nitrosylated after NOC7 application, and found that RyR1 *S*-nitrosylation also occurred in cerebellar slice preparations (Supplementary Figure S1F and G).

There was a marked difference in the time-course of NOC7-induced Ca^{2+} responses between PCs in slice preparations and HEK293 cells. However, the difference can (at least in part) be accounted for by the lag time in the increase in NOC7 concentration around the neurons, because the NO donor was applied by superfusion of thick slice preparations. In accordance with this notion, the time course of NICR in response to 300 μM NOC7 in cultured cerebral neurons was similar to that of HEK293 cells (Figure S1H vs. Figure S2G top left panel).

NO-induced Ca^{2+} release is induced by neuronal activity

Having shown that exogenous NO induces NICR in RyR1-expressing cells, we then studied

whether NICR is evoked by endogenous NO signaling in the brain. When physiologically relevant burst stimulations (BS; 5 pulses at 50 Hz) (Chadderton et al, 2004) are repeatedly applied, parallel fibers (PFs) generate local NO signals near the PF-PC synapses that reach micromolar concentrations in acute cerebellar slices (Namiki et al, 2005). Thus, we assessed $[Ca^{2+}]_i$ in PC dendrites receiving intrinsic NO signaling from PFs. Stimulus intensity was adjusted to ensure that glutamatergic Ca^{2+} responses to a single BS were negligible in postsynaptic PC dendrites (Supplementary Figure S3A). A gradual increase in Ca^{2+} was observed in PC dendrites after repetitive application of BS to PFs at 1 Hz for 60 s (Figure 3A–C), and $[Ca^{2+}]_i$ slowly decreased after termination of BS (Figure 3C). The magnitude of the BS-induced Ca^{2+} response was comparable with that of the glutamatergic response observed with a high-frequency PF input, but the time course of the BS response was much slower (Supplementary Figure S3B vs. C). The BS-induced Ca^{2+} signal was localized on the dendrites near the stimulation electrode (Figure 3A and B), similar to the PF-derived NO signal (Namiki et al, 2005). Depletion of Ca^{2+} stores by thapsigargin abolished the Ca^{2+} increase (Figure 3C and E). Treatment with the IP_3R inhibitor heparin via a patch pipette had no effect on the BS-induced Ca^{2+} increase (Figure 3E; Supplementary Figure S3D), even though the concentration of heparin (4 mg ml^{-1}) used was sufficient to inhibit metabotropic glutamate receptor (mGluR)-mediated, IP_3-dependent Ca^{2+} release in PCs (Supplementary Figure S3B). The inhibitory effect of heparin on IP_3-dependent Ca^{2+} release was corroborated by another report (Takechi et al, 1998). Conversely, BS-induced Ca^{2+} signaling was blocked by dantrolene (Figure 3D and E). These results indicate that the

BS-induced slow $[Ca^{2+}]_i$ increase is dependent on Ca^{2+} release via RyR. Glutamatergic signaling is unlikely to be involved, because the BS-induced Ca^{2+} release was observed in the presence of both ionotropic and metabotropic glutamate receptor antagonists, NBQX (2,3-Dioxo-6-nitro-1,2,3,4-tetrahydrobenzo[f]quinoxaline-7-sulfonamide) and CPCCOEt (7-(Hydroxyimino)cyclopropa[*b*]chromen-1α-carboxylate ethyl ester), respectively (Figure 3E; Supplementary Figure S3G). We confirmed that these glutamate receptor antagonists inhibit glutamatergic Ca^{2+} responses in PCs (Supplementary Figure S3B). Furthermore, an NMDA receptor inhibitor, AP5 (D-(-)-2-amino-5-phosphonopentanoic acid), did not have any effect on the BS-induced Ca^{2+} release (Supplementary Figure S3H).

We also examined if NO is causally involved in the BS-induced Ca^{2+} release. We found that the NOS inhibitor, L-NAME (N^G-Nitro-L-arginine methyl ester), completely blocked the BS-induced Ca^{2+} release (Figure 3E; Supplementary Figure S3I). We also studied mutant mice deficient in NOS1 (Huang et al, 1993). The BS-induced NO signal in PCs measured using a NO probe (HBR-GFP) (Namiki et al, 2005) was found to be absent in *Nos1*$^{-/-}$ mice, indicating that NOS1 is the dominant source of NO upon PF stimulation (Supplementary Figure S3M). Additionally, there was no $[Ca^{2+}]_i$ increase in response to BS in the PCs of *Nos1*$^{-/-}$ mice (Figure 3C and E), even though an exogenous NO source, NOC7 (30 and 300 μM), induced a significant $[Ca^{2+}]_i$ increase, which is comparable with that in *Nos1*$^{+/+}$ mice (Supplementary Figure S3P). Thus, BS-induced Ca^{2+} release is dependent on NOS1-induced NO generation. ODQ (1 and 10 μM) had no inhibitory effects on BS-induced Ca^{2+} release (Figure 3E; Supplementary Figure S3E and F). In addition,

ascorbic acid (which has been used for selective reduction of cysteine *S*-nitrosothiols (Burgoyne & Eaton, 2010; Jaffrey et al, 2001)) applied to PCs through the patch pipette abolished BS-induced Ca^{2+} release (Figure S3J). These findings are consistent with the involvement of *S*-nitrosylation, rather than sGC-cGMP signaling, in BS-induced Ca^{2+} release. Furthermore, there were no significant changes in the BS-induced Ca^{2+} release in *Ryr3*$^{-/-}$ mice (Supplementary Figure S3K). Taken together, these findings indicate that PFs stimulated in a physiological manner generate NO, which in turn induces NICR via RyR1 in PCs.

Critical role of NICR in cerebellar long-term potentiation

We next studied the potential physiological or pathophysiological roles of NICR. BS-induced NO generation by PFs also induces long-term potentiation (LTP) in the PF-PC synapse (Namiki et al, 2005). This form of LTP is similar to PF-LTP, generated by PF stimulation at 1 Hz for 5 min (Coesmans et al, 2004; Lev-Ram et al, 2002), in that both are generated postsynaptically and are NO-dependent, although they are not cGMP-dependent. PF-LTP is dependent upon the level of $[Ca^{2+}]_i$ in PC dendrites (Coesmans et al, 2004). Confirming that PF stimulation at 1 Hz for 5 min induces LTP (Figure S4K), we measured $[Ca^{2+}]_i$ in PC dendrites during PF stimulation at 1 Hz. We observed an increase in $[Ca^{2+}]_i$ with a peak amplitude comparable with that during BS stimulation (Figure S3L). Consideration of these previous findings and our findings suggests that NICR may be involved in synaptic plasticity, and we tested this possibility.

Repeated BS (60 times at 1 Hz) applied to PFs induced a significant potentiation in PF-PC synapses that lasted >30 min (Figure 4A). This LTP was absent in *Nos1*$^{-/-}$ mice (Figure 4A and C), although LTP in the *Nos1*$^{-/-}$ cerebellum could be induced by NOC7 as in wild-type animals (Figure S4L). Furthermore, ODQ (10 μM) had no inhibitory effect (Supplementary Figure S4G), although 1 μM of ODQ was sufficient to inhibit long-term depression (LTD) in the same synapse of the cerebellar slice preparations (Supplementary Figure S4M and N), which is known to be dependent upon cGMP signaling (Ito, 2002). These results confirm that BS-induced LTP is NO-dependent but not cGMP-dependent. Consistent with the central role of NO in LTP induction, mGluR or NMDA receptor blockade did not have a significant effect on LTP (Figure 4C; Supplementary Figure S4E and F). We then tested if intracellular Ca^{2+} release has a role in the induction of LTP. Indeed, depletion of intracellular Ca^{2+} stores by thapsigargin abolished LTP (Figure 4C; Supplementary Figures S4B and L). Furthermore, dantrolene applied in the bath or intracellularly to PCs through a patch pipette blocked LTP (Figure 4B and C; Supplementary Figure S4C), whereas intracellular application of heparin to PCs had no significant effect (Figure 4C; Supplementary Figure S4D). These findings indicate that Ca^{2+} release via RyR, but not IP_3R, is required for the induction of LTP. We also found that the *S*-nitrosylation decomposer ascorbic acid blocked LTP (Figure S4H). Although the dominant RyR subtype in PCs is RyR1, RyR3 is also expressed. However, cerebellar LTP was similarly induced in slice preparations of *Ryr3*$^{-/-}$ mice (Supplementary Figure S4I). Intracellular application of a Ca^{2+} buffer, BAPTA (5–30 mM), to PCs through a patch

pipette inhibited LTP in a concentration-dependent manner (Figure 4C; Supplementary Figure S4J). Although LTP was observed in the presence of 5 mM BAPTA, 10 mM BAPTA was sufficient to inhibit LTP. The concentration-dependent effect of BAPTA on LTP suggests that local Ca^{2+} signaling rather than a global increase in the dendritic $[Ca^{2+}]_i$ is required for LTP induction (see Discussion). Taken together, these findings indicate that NICR via the RyR1 in PCs is essential for inducing LTP in PF-PC synapses of the cerebellum.

Involvement of NICR in neuronal cell death

Cerebral ischemia causes NOS-dependent NO generation. NOS1-dependent NO generation is implicated in ischemic brain injury, whereas NO generation by type 3 (or endothelial) NOS is considered beneficial to brain injury because it increases blood flow (Iadecola, 1997). Indeed, brain injury after middle cerebral artery occlusion (MCAO) is significantly milder in mice treated with a NOS1-specific inhibitor and in *Nos1*$^{-/-}$ mice (Huang et al, 1994). The NO concentration reaches micromolar levels in ischemic cerebral tissue during and after MCAO (Malinski et al, 1993). Such NO signaling during ischemia is expected to activate NICR in neurons. We therefore examined whether or not NICR is involved in NOS1-dependent brain injury.

We first used a mouse MCAO model to examine the potential role of NICR in ischemic brain injury. In line with another study (Huang et al, 1994), ischemic brain injury in the MCAO model was milder in *Nos1*$^{-/-}$ mice than in *Nos1*$^{+/+}$ mice (Figure 5A and B). We then

examined the effects of the NICR inhibitor dantrolene, and found that subarachnoidal administration of dantrolene after reperfusion of MCAO had a protective effect on MCAO-induced brain injury in *Nos1*$^{+/+}$ mice (Figure 5A and B). These findings are corroborated by similar findings in other animal models (Li et al, 2005). Conversely, there was very little effect of dantrolene on infarction volume in *Nos1*$^{-/-}$ mice (Figure 5B). These results suggest that NOS1-dependent NICR may play a role in ischemic brain injury following reperfusion in the MCAO model.

We next analyzed the potential role of NICR in NO-induced neuronal cell death in culture. NOC12 (a sister NO donor with a longer half-life than NOC7) was used to mimic a prolonged increase in NO concentrations during brain ischemia (Malinski et al, 1993) (see Supplementary materials and methods). NOC12 induced an increase in $[Ca^{2+}]_i$ in cerebral neurons of wild-type mice (Figure 6A Left). The $[Ca^{2+}]_i$ increase was observed in the absence of extracellular Ca^{2+}, and was abolished in the presence of dantrolene (Figure 6B) or in cerebral neurons from *Ryr1*$^{-/-}$ mice (Figure 6A Right). We thus confirmed the presence of NICR in cerebral neurons. When we examined neuronal cell death after application of NOC12, there was a significant increase in cerebral neuron death 16 h after the NO donor treatment (Figure 6C and D). However, in the presence of dantrolene, NO donor-induced neuronal cell death was significantly attenuated (Figure 6C and D). These results suggest that NICR is (at least in part) involved in NO-induced neuronal cell death. Dantrolene may have effects other than NICR inhibition, so we further studied the role of NICR in neuronal cell death using cerebral neurons obtained from *Ryr1*$^{-/-}$ mice (Figure 6A Right). Consistent

with the notion that NICR is involved in NO-induced cell death, cell death was significantly lower in *Ryr1*$^{-/-}$ neurons compared with *Ryr1*$^{+/+}$ neurons (Figure 6C and D). In addition, dantrolene had no protective effect on NO donor-induced cell death in *Ryr1*$^{-/-}$ neurons (Figure 6C and D). Taken together, these findings suggest that NICR via RyR1 contributes to NO-induced neuronal cell death.

The potential importance of *S*-nitrosylation of RyR1 in NO-induced cell death was examined in HEK cells expressing extrinsic RyR1. NOC12 application induced a dose-dependent increase in $[Ca^{2+}]_i$ in cells expressing RyR1, but not in cells expressing C3635A-RyR1 (Figure S5A), as in the case of NOC7 (Figure 2C). The NOC12-induced Ca^{2+} increase was abolished by 10 μM ryanodine (Figure S5B). We then analyzed the effect of NOC12 on cell viability using the MTT assay 16 h after the NO donor treatment. NOC12 induced dose-dependent suppression of cell viability in cells expressing wild-type RyR1 (Figure S5C). Although the same effect of anisomycin on cell viability was observed in cells expressing RyR1 or C3635A-RyR1, the effect of NOC12 was significantly attenuated in cells expressing C3635A-RyR1 at 2 mM and 3 mM NOC12, but not at 1 mM NOC12, where Ca^{2+} release was not observed (Figure S5C). Furthermore, dantrolene, which blocks NOC12-induced Ca^{2+} increase (Figure S6B), showed a protective effect against 3 mM NOC12-induced cell viability loss in cells expressing wild-type RyR1, but not in cells expressing C3635A-RyR1 (Figure S6C). These results support the notion that *S*-nitrosylation-dependent NICR is one of the regulators of cell viability.

Discussion

In the present study, it was found that NO induces Ca^{2+} release via RyR1 in central neurons. The agonistic effect of NO on intracellular Ca^{2+} release is mediated by *S*-nitrosylation of RyR1, in particular at cysteine 3635 of the Ca^{2+} release channel in an extrinsic expression system. The same mechanism may underlie the NO-induced Ca^{2+} responses in neurons, although confirmation is required. The modulation of Ca^{2+} release via *S*-nitrosylation of RyR1 has been implicated in skeletal muscle contractions in low PO_2 and pathological conditions (Bellinger et al, 2009; Durham et al, 2008; Eu et al, 2003). Thus, although RyR1 is primarily regulated by voltage-gated Ca^{2+} channels through direct protein–protein interactions in skeletal muscle cells, NO-induced *S*-nitrosylation of RyR1 has a modulatory, enhancing effect on Ca^{2+} release in these cells. However, the tight regulation of RyR1 via Ca^{2+} channels, as seen in skeletal muscle cells, has not yet been demonstrated in central neurons (Kano et al, 1995). In contrast to the rapid and transient RyR1-mediated Ca^{2+} release events as seen during twitch and tetanus contractions in skeletal muscle, NICR induced by synaptic input in central neurons produces a much slower and prolonged increase in $[Ca^{2+}]_i$. It remains to be elucidated if NO has a similar direct Ca^{2+}-releasing effect via RyR1 outside the brain, where the time-course of NICR can be influenced by many factors. These include the expression levels of RyR1 and SERCA, the time-course of NO increase, and the rate of removal of *S*-nitrosylation.

Other subtypes of RyR, RyR2 and RyR3 are also expressed in the brain. It was found that RyR3 also mediates NICR. RyR1 is the most dominant RyR subtype found in cerebellar

PCs (Furuichi et al, 1994; Giannini et al, 1995; Mori et al, 2000; Sawada et al, 2008), and it is likely that this subtype mediates NICR and LTP in these cells. Supporting this notion, PCs of *Ryr3*$^{-/-}$ mice demonstrated BS-induced NICR and LTP, whose levels were comparable with that of wild-type mice (Supplementary Figure S3K and S4I). Despite this, it remains to be examined whether NICR via RyR3 has physiological and pathophysiological roles in other regions of the brain.

Unlike RyR1 in skeletal muscle, RyR2 is regulated by the CICR mechanism in cardiac muscle. Corroborating the results of another report (Sun et al, 2008), there was virtually no direct effect of NO on Ca^{2+} release via RyR2 (Figure 2B). Given that the important cysteine residue (i.e. cysteine 3635 of RyR1) is conserved among all RyR subtypes (Supplementary Figure S2H), subtype specificity in NICR is remarkable. Thus, the three-dimensional structure around the critical cysteine residue may be important for *S*-nitrosylation or channel gating. However, this mechanism requires further clarification. Interestingly, RyR2 can be activated by *S*-nitrosoglutathione, which can also be formed in the brain (Kluge et al, 1997; Sun et al, 2008). Dantrolene, which does not block RyR2 (Zhao et al, 2001), abolished NICR and LTP in PCs, so *S*-nitrosoglutathione-mediated RyR2 activation is not likely to play a major part in the neuronal functions explored in the present study.

NICR is induced by mimicking physiological patterns of neuronal activity, and is essential in inducing cerebellar LTP, which is the reverse process of cerebellar LTD (Coesmans et al, 2004; Lev-Ram et al, 2003). Cerebellar LTP has also been implicated in the memory of fear (Sacchetti et al, 2004). As to the molecular mechanism of LTP,

N-ethylmaleimide-sensitive factor (NSF)-dependent recruitment of AMPAR in the postsynaptic membrane has been shown to underlie cerebellar LTP (Kakegawa & Yuzaki, 2005). Furthermore, *S*-nitrosylation of NSF promotes the surface expression of AMPA receptors in central neurons (Huang et al, 2005). These previous results indicate that NSF is an important target of NO in cerebellar LTP induction. Cerebellar LTP depends not only on NO but also on the level of $[Ca^{2+}]_i$ in PCs (Coesmans et al, 2004). However, the relationship between these signals is incompletely understood. NICR is a plausible candidate that links NO and $[Ca^{2+}]_i$. In general agreement with this notion, intracellular application of BAPTA (5–30 mM) to PCs had a dose-dependent inhibitory effect on LTP (Figure S4J). Interestingly, 5 mM BAPTA was not sufficient to inhibit LTP, in line with the successful generation of 1 Hz-LTP in the presence of 5 mM BAPTA (Lev-Ram et al, 1995). The absence of an inhibitory effect of 5 mM BAPTA on LTP may be partly explained by prevention of residual LTD (Lev-Ram et al, 1995). Because 5 mM BAPTA is expected to inhibit a global increase in the dendritic $[Ca^{2+}]_i$, the result may also suggest involvement of local Ca^{2+} signaling in the generation of LTP. Single-channel openings of RyR1 and RyR2 generate ionic currents of ~0.5 pA under near-physiological ionic conditions (Kettlun et al, 2003). These unitary events would generate a localized increase in Ca^{2+} concentration around the RyR. A recent study showed that the Ca^{2+} binding rate constants of calmodulin are so high that calmodulin can effectively "trap" Ca^{2+} immediately when Ca^{2+} enters the cytoplasm before it binds to cytoplasmic Ca^{2+} buffers (Faas et al, 2011). Therefore, if calmodulin or other Ca^{2+}-binding proteins with similar Ca^{2+}-binding properties are involved in the signaling process

downstream of the Ca^{2+} release from the RyR, it is possible that lower concentrations of BAPTA cannot completely block the process. An example can be found in cardiac cells, in which RyR2 and L-type Ca^{2+} channels localize closely together at the junction between the sarcoplasmic reticulum and plasma membrane. L-type Ca^{2+} channels undergo inactivation in response to an increase in $[Ca^{2+}]_i$ through a calmodulin-dependent mechanism (Peterson et al, 1999; Zühlke et al, 1999). Ca^{2+} release from RyR2 facilitates the Ca^{2+}-dependent inactivation of L-type Ca^{2+} channels, and the extent of facilitation is suppressed by intracellular application of BAPTA (3 and 10 mM) in a concentration-dependent manner. However, a considerable fraction of Ca^{2+} release-dependent inactivation remains even in the presence of BAPTA: about 61% and 32% of control with 3 and 10 mM BAPTA, respectively, at –20 mV (Sham, 1997). Under this experimental condition, RyR2 is activated by Ca^{2+} influx through L-type Ca^{2+} channels, so BAPTA also inhibits the activation of RyR2 itself. Therefore, the inhibitory effect of BAPTA on Ca^{2+} release-induced L-type Ca^{2+} channel inactivation *per se* is overestimated. These considerations suggest that close localization of RyR1 and downstream signal transduction molecules may be involved in the generation of LTP. Of course, this mechanism requires further clarification. Taken together, RyR1 is very likely to be another essential target of NO in cerebellar LTP induction. NOS1 and RyR1 are co-expressed in various regions of the brain, so NICR may have additional physiological roles in the brain.

NO is implicated in various pathological conditions, including ischemic brain injury, via the generation of reactive nitrogen species such as peroxynitrite (Pacher et al, 2007).

Our results suggest that NICR via RyR1 is also involved in NO-induced cell death in cerebral neurons in culture. The NO-induced neuronal cell death was significantly milder in *RyR1*$^{-/-}$ neurons, in which NICR was absent. In addition, the NO-induced neuronal cell death was attenuated by dantrolene (which inhibits NICR), and the protective effect of dantrolene was absent in *Ryr1*$^{-/-}$ neurons. Dantrolene also had a protective effect on ischemic brain injury in the MCAO model. Taken together, these findings suggest that NOS1-dependent NO generation may exert its adverse effects in ischemic neuronal cell death, in part, via NICR, causing either an excessive increase in neuronal Ca^{2+} concentrations or depleting intracellular Ca^{2+} stores, which in turn stresses the endoplasmic reticulum (Li et al, 2005). We studied the importance of cysteine 3635 of RyR1 in cell viability in HEK-293 cells. The results suggested that the cysteine residue is one of the important factors in NO-induced cell death. To corroborate the notion of the involvement of NICR in ischemic neuronal cell death, we tried to measure *S*-nitrosylation levels of RyR1 in the cerebral cortex. Thus far, the measurement has been difficult because the level of protein expression of RyR1 in the mouse cerebral cortex is not sufficiently high for reliable determination with the biotin switch method. A new detection method with a higher sensitivity is needed, and this issue should be addressed in future studies. Ischemic brain injury is a complex process, and the roles of NICR in the disease process require further clarification. With this reservation, it seems possible that drugs that inhibit NICR may have therapeutic value in some forms of ischemic brain injury.

Materials and methods

Experiments using animals

All animal-related procedures were in accordance with the guidelines of The University of Tokyo (Tokyo, Japan).

Slice preparation and whole-cell patch-clamp recording

C57BL/6 mice (postnatal days 24–32) were sacrificed by cervical dislocation under anesthesia with diethyl ether. The cerebellum was excised, and parasagittal cerebellar slices (250-μm thick) prepared from the vermis (Edwards et al, 1989; Kakizawa et al, 2005; Kakizawa et al, 2000). *Nos1*$^{-/-}$ and *Nos1*$^{+/-}$ mice (Huang et al, 1993) were obtained from The Jackson Laboratory. In experiments using *Ryr1*$^{-/-}$ mice, cerebellar slices were prepared from neonatal animals because of the neonatal lethality of these mice (Takeshima et al, 1994). *Ryr3*$^{-/-}$ mice were also used (Takeshima et al, 1996). Whole-cell recordings were obtained from visually identified PCs under an upright microscope (BX51WI, Olympus, Tokyo, Japan) using a 40× water-immersion objective at room temperature (23–25°C), with the exception of experiments that used dantrolene (36 ± 1°C). The resistance of the patch pipettes was 2.0–3.5 MΩ when filled with an intracellular solution (in mM) composed of: 130 K-gluconate, 10 KCl, 10 NaCl, 1 EGTA, 4 ATP-Mg, 0.4 GTP-Na and 10 HEPES (pH 7.3; adjusted with KOH). The standard bathing solution (in mM) was composed of: 125 NaCl, 2.5 KCl, 2 $CaCl_2$, 1 $MgSO_4$, 1.25 NaH_2PO_4, 26 $NaHCO_3$, and 20 glucose, bubbled

with 95% CO_2 and 5% CO_2. Bicuculline (10 μM) was always added to block the inhibitory postsynaptic currents.

Ca^{2+} imaging in slice preparations

For intracellular Ca^{2+} imaging in PCs, a Ca^{2+}-sensitive dye, Oregon Green 488 BAPTA-1 (100 μM), was introduced into PCs through the patch pipette, and the concentration of EGTA in the pipette solution was decreased to 0.5 mM. Five-to-nine sequential confocal images (excitation at 488 nm), obtained at 3–4 μm z-axis intervals, were acquired every 0.8 s using an upright microscope (BX51WI; Olympus) equipped with a confocal scanning unit and an argon laser (FV300, Olympus), and projected onto a plane to obtain dendrite images at 10-s or 5-s intervals.

Electrophysiological measurements

For focal stimulation of PFs, a stimulation pipette (tip diameter, 5–10 μm) was filled with standard bathing solution and used to apply square pulses (0.1 ms in duration, 0–20 V in amplitude) to the molecular layer, specifically in the middle portion of the molecular layer approximately one-third of the distance below the pial surface. The intensity of each stimulus was adjusted to evoke PF-EPSCs with an amplitude of 60–120 pA. The ionic current was recorded from PCs using a patch-clamp amplifier (EPC-9, HEKA, Lambrecht/Pfalz, Germany) at a holding potential of –90 or –80 mV, after compensating for the liquid junction potential. The signals were filtered at 2 kHz and digitized at 20 kHz.

Expression of exogenous RyR1, RyR2 and RyR3 in HEK293 cells

Full-length RyR1 cDNA (Takeshima et al, 1989) was subcloned into the multiple cloning sites (MCS) of the pcDNA/FRT/TO expression vector (Invitrogen, Carlsbad, CA, USA) that was modified by the addition of a Nhe I site. Tetracycline-inducible stable HEK293 cell lines were generated using the Flp-In T-REx system according to manufacturer's instructions. RyR2 cDNA (Nakai et al, 1990) was similarly subcloned into the pcDNA/FRT/TO vector, and stable HEK293 cell lines obtained (Chugun et al, 2007). RyR3 cDNA (Chen et al, 1997) (a kind gift from Dr. SR Chen, University of Calgary, Alberta, Canada) was similarly expressed in HEK293 cells. Flp-In™-293 HEK293 cells were cultured on collagen-coated dishes in Dulbecco's modified Eagle's medium (DMEM) supplemented with 10% fetal bovine serum, penicillin (100 U/ml), streptomycin (100 U/ml) and 2 mM glutamine. HEK293 cells at passages from 10 to 20 were plated onto collagen-coated glass-bottom dishes 3 d prior to Ca^{2+} imaging. The generation of C3635A-RyR1 is described in Supplementary materials and methods.

Cerebral neuron culture

Neurons were prepared from the cerebral cortices of wild-type or *Ryr1*$^{-/-}$ mice fetuses [embryonic day 16 (E16) or E19] based on a modification of a previously described procedure (Kanemaru et al, 2007). Briefly, minced cerebral cortices were treated with 2.5% trypsin (Invitrogen) and 0.1% DNase I (Sigma–Aldrich, St Louis, MO, USA) in

Ca^{2+}/Mg^{2+}-free phosphate-buffered saline (PBS) for 3 min at room temperature. Cells were washed with Neurobasal-A medium (Invitrogen) supplemented with 5% fetal calf serum, penicillin (100 U/ml), streptomycin (100 U/ml), and 2 mM L-glutamine (Sigma–Aldrich) and dissociated by triturating with a fire-polished Pasteur pipette in Ca^{2+}/Mg^{2+}-free PBS containing 0.05% DNase I and 0.03% trypsin inhibitor (Sigma–Aldrich). Dispersed cells were plated at 5.0–9.0 $\times$ 10^4 cells cm^{-2} on glass coverslips that had been coated with poly-L-lysine (Sigma–Aldrich) and mouse laminin (Invitrogen). Cells were then cultured at 37°C in Neurobasal-A (Invitrogen) with B-27 supplement (Invitrogen), penicillin (100 U/ml), streptomycin (100 U/ml), and 2 mM L-glutamine under a humidified atmosphere containing 5% CO_2. Culture medium contained 5% fetal calf serum for the first day after plating. The medium was then changed every 2 d by replacing half of the old medium with fresh medium. Cells cultured for 5–20 d were plated onto poly-L-lysine- and laminin-coated glass coverslips 7–15 d prior to Ca^{2+} imaging. Immediately before Ca^{2+} imaging in cultured neurons, $CaCl_2$ in physiological salt solution (PSS) was replaced with equimolar $MgCl_2$ to inhibit spontaneous activity.

Ca^{2+} imaging in cultured cells

Cells were loaded at room temperature with 4 μM fura-2 AM in PSS (in mM) containing: 150 NaCl, 4 KCl, 2 $CaCl_2$, 1 $MgCl_2$, 5.6 glucose and 10 HEPES at pH 7.4. Fluorescence images were acquired at >420 nm using an inverted microscope equipped with a cooled CCD camera at a rate of one frame every 1 s or 2 s. Excitation wavelengths were 345 nm

and 380 nm. Ca^{2+} imaging experiments were conducted at room temperature, with the exception of the experiments conducted with dantrolene (35 ± 1°C). Image analyses were carried out using IPLab software (BD Biosciences Bioimaging, Rockville, MD, USA). Regions of interest (ROIs) corresponding to individual cells were selected and the mean fluorescence intensity (*F*) of each ROI minus the background intensity was calculated for each frame. We used the F_{345}/F_{380} ratio (the value of *F* at an excitation wavelength of 345 nm divided by the value of *F* at an excitation wavelength of 380 nm) to estimate $[Ca^{2+}]_i$, as described elsewhere (Grynkiewicz et al, 1985). The K_d (239 nM) for Ca^{2+} was determined via *in vitro* calibration of fura-2 fluorescence.

Analyses of NO-induced neuronal cell death

Primary cultured neurons were exposed to 500 μM NOC12 or vehicle, with or without 10 μM dantrolene, and cultured at 37°C. After 16 h, primary cultures were stained with 0.2 μM calcein-AM, 1 μM propidium iodide (PI), and 0.4 μM Hoechst 33342 for 10 min at room temperature. Fluorescence images were obtained at >420 nm (excitation at 350 nm) for Hoechst 33342, 515–550 nm (excitation 480 nm) for calcein, and >600 nm (excitation 540 nm) for PI using an inverted microscope (IX70; Olympus) equipped with a 40× (N.A. = 0.7) or 10× (N.A. = 0. 4) objective and a CCD camera. Cell death was expressed as the number of PI-positive cells divided by the number of total cells (Hoechst 33342-positive cells). High-content single-cell image analyses were undertaken using CellProfiler (Carpenter et al, 2006).

Biotin switch method

S-nitrosylation of RyR1 in HEK293 cells and in cerebellar slice preparations was detected via the biotin switch method (Ckless et al, 2004; Jaffrey & Snyder, 2001). This method utilizes a *S*-nitrosylated protein detection assay kit (Cayman Chemical, Ann Arbor, MI, USA) with some modifications, as described in Supplementary materials and methods.

Middle cerebral artery occlusion (MCAO) model

Male 8–12-week-old *Nos1*$^{-/-}$ mice and their wild-type littermates weighing 20–30 g at the time of surgery were used. Anesthesia was maintained during surgery with 1.5% isoflurane in a 30% O_2/70% N_2O gas mixture. Rectal and occipitocervical muscular temperatures were maintained at 37 ± 0.3°C using a heating blanket and lamp. After recovery from anesthesia, mice were placed in an incubator at 33°C and 50% humidity to prevent hypothermia, and provided with food and water *ad libitum*. The methodology for generating the MCAO mouse model has been described previously (Chen et al, 2008), and is briefly described in the Supplementary materials and methods.

Determination of the infarct volume

After 24 h of reperfusion, mice were deeply anesthetized and intracardially perfused with heparinized saline. Brains were extracted and 2-mm coronal sections cut. Individual sections were incubated for 20 min in 2% triphenyltetrazolium chloride (TTC) in PBS at 37°C. The

TTC was drained and slices placed in 10% formalin for 30 min. Images of the slices were acquired using a digital camera. Infarct volume was calculated by two members blinded to the study protocol using the Leach correction (Leach et al, 1993):

[Lesion area of each section] = [Ipsilateral lesion area] × ([Contralateral hemisphere area] / [Ipsilateral hemisphere area]).

Lesion volume was calculated as the sum of the lesioned areas in all five sections and multiplied by slice thickness (2 mm).

Supplementary data

Supplementary data are available at *The EMBO Journal* Online (http://www.embojournal.org).

Acknowledgements

This work was supported by a Grant-in-Aid for Scientific Research and a Global COE Program entitled “Integrative Life Science Based on the Study of Biosignaling Mechanisms” from MEXT (Japan), as well as grants from the Uehara Memorial Foundation, Takeda Science Foundation, Mochida Memorial Foundation, and the Suzuken Memorial Foundation.

Author contributions: SK, TY and MI designed the research; SK, TY, YC, AI, TM, HO

and HT carried out the experiments; NK, OS, MW, NM, KO, TS and NS provided new experimental tools; SK, TY, YC, AI, TM and MI analyzed the data; SK and MI wrote the manuscript; and MI supervised the study.

Conflict of interest

The authors declare that they have no conflict of interest.

References

Aghdasi B, Reid MB, Hamilton SL (1997) Nitric oxide protects the skeletal muscle Ca^{2+} release channel from oxidation induced activation. *J Biochem* 272: 25462-25467

Bellinger AM, Reiken S, Carlson C, Mongillo M, Liu X, Rothman L, Matecki S, Lacampagne A, Marks AR (2009) Hypernitrosylated ryanodine receptor calcium release channels are leaky in dystrophic muscle. *Nat Med* 15: 325-330

Berridge MJ, Lipp P, Bootman MD (2000) The versatility and universality of calcium signalling. *Nat Rev Mol Cell Biol* 1: 11-21

Bredt DS, Glatt CE, Hwang PM, Fotuhi M, Dawson TM, Snyder SH (1991) Nitric oxide synthase protein and mRNA are discretely localized in neuronal populations of the mammalian CNS together with NADPH diaphorase. *Neuron* 7: 615-624

Bredt DS, Snyder SH (1994) Nitric oxide: a physiologic messenger molecule. *Annu Rev Biochem* 63: 175-195

Burgoyne JR, Eaton P (2010) A Rapid Approach for the Detection, Quantification, and Discovery of Novel Sulfenic Acid or S-Nitrosothiol Modified Proteins Using a Biotin-Switch Method. *Mehtod Enzymol* 473: 281-303

Carpenter AE, Jones TR, Lamprecht MR, Clarke C, Kang IH, Friman O, Guertin DA, Chang JH, Lindquist RA, Moffat J, Golland P, Sabatini DM (2006) CellProfiler: image analysis software for identifying and quantifying cell phenotypes. *Genome Biol* 7: R100

Chadderton P, Margrie TW, Hausser M (2004) Integration of quanta in cerebellar granule cells during sensory processing. *Nature* 428: 856-860

Chen SR, Li X, Ebisawa K, Zhang L (1997) Functional characterization of the recombinant type 3 Ca^{2+} release channel (ryanodine receptor) expressed in HEK293 cells. *J Biol Chem* 272: 24234-24246

Chen Y, Ito A, Takai K, Saito N (2008) Blocking pterygopalatine arterial blood flow decreases infarct volume variability in a mouse model of intraluminal suture middle

cerebral artery occlusion. *J Neurosci Meth* 174: 18-24

Chugun A, Sato O, Takeshima H, Ogawa Y (2007) Mg^{2+} activates the ryanodine receptor type 2 (RyR2) at intermediate Ca^{2+} concentrations. *Am J Physiol Cell Physiol* 292: C535-544

Ckless K, Reynaert NL, Taatjes DJ, Lounsbury KM, van der Vliet A, Janssen-Heininger Y (2004) In situ detection and visualization of S-nitrosylated proteins following chemical derivatization: identification of Ran GTPase as a target for S-nitrosylation. *Nitric Oxide* 11: 216-227

Coesmans M, Weber JT, De Zeeuw CI, Hansel C (2004) Bidirectional parallel fiber plasticity in the cerebellum under climbing fiber control. *Neuron* 44: 691-700

Durham WJ, Aracena-Parks P, Long C, Rossi AE, Goonasekera SA, Boncompagni S, Galvan DL, Gilman CP, Baker MR, Shirokova N, Protasi F, Dirksen R, Hamilton SL (2008) RyR1 S-nitrosylation underlies environmental heat stroke and sudden death in Y522S RyR1 knockin mice. *Cell* 133: 53-65

Edwards FA, Konnerth A, Sakmann B, Takahashi T (1989) A thin slice preparation for patch clamp recordings from neurones of the mammalian central nervous system. *Pflugers Arch* 414: 600-612

Endo M (2009) Calcium-induced calcium release in skeletal muscle. *Physiol Rev* 89: 1153-1176

Eu JP, Hare JM, Hess DT, Skaf M, Sun J, Cardenas-Navina I, Sun QA, Dewhirst M, Meissner G, Stamler JS (2003) Concerted regulation of skeletal muscle contractility by oxygen tension and endogenous nitric oxide. *Proc Natl Acad Sci USA* 100: 15229-15234

Eu JP, Sun J, Xu L, Stamler JS, Meissner G (2000) The skeletal muscle calcium release channel: coupled O_2 sensor and NO signaling functions. *Cell* 102: 499-509

Faas GC, Raghavachari S, Lisman JE, Mody I (2011) Calmodulin as a direct detector of Ca^{2+} signals. *Nat Neurosci* 14: 301-304

Furuichi T, Furutama D, Hakamata Y, Nakai J, Takeshima H, Mikoshiba K (1994) Multiple types of ryanodine receptor/Ca^{2+} release channels are differentially expressed in rabbit brain. *J Neurosci* 14: 4794-4805

Giannini G, Conti A, Mammarella S, Scrobogna M, Sorrentino V (1995) The ryanodine receptor/calcium channel genes are widely and differentially expressed in murine brain and peripheral tissues. *J Cell Biol* 128: 893-904

Grynkiewicz G, Poenie M, Tsien R (1985) A new generation of Ca^{2+} indicators with greatly improved fluorescence properties. *J Biol Chem* 260: 3440-3450

Hess DT, Matsumoto A, Kim SO, Marshall HE, Stamler JS (2005) Protein *S*-nitrosylation: purview and parameters. *Nat Rev Mol Cell Biol* 6: 150-166

Huang PL, Dawson TM, Bredt DS, Snyder SH, Fishman MC (1993) Targeted disruption of the neuronal nitric oxide synthase gene. *Cell* 75: 1273-1286

Huang Y, Man HY, Sekine-Aizawa Y, Han Y, Juluri K, Luo H, Cheah J, Lowenstein C, Huganir RL, Snyder SH (2005) S-nitrosylation of N-ethylmaleimide sensitive factor mediates surface expression of AMPA receptors. *Neuron* 46: 533-540

Huang Z, Huang PL, Panahian N, Dalkara T, Fishman MC, Moskowitz MA (1994) Effects of cerebral ischemia in mice deficient in neuronal nitric oxide synthase. *Science* 265: 1883-1885

Iadecola C (1997) Bright and dark sides of nitric oxide in ischemic brain injury. *Trends Neurosci* 20: 132-139

Ito M (2002) The molecular organization of cerebellar long-term depression. *Nat Rev Neurosci* 3: 896-902

Jaffrey SR, Erdjument-Bromage H, Ferris CD, Tempst P, Snyder SH (2001) Protein S-nitrosylation: a physiological signal for neuronal nitric oxide. *Nature cell biology* 3: 193-197

Jaffrey SR, Snyder SH (2001) The biotin switch method for the detection of S-nitrosylated

proteins. *Sci STKE* 2001: PL1

Kakegawa W, Yuzaki M (2005) A mechanism underlying AMPA receptor trafficking during cerebellar long-term potentiation. *Proceedings of the National Academy of Sciences of the United States of America* 102: 17846-17851

Kakizawa S, Miyazaki T, Yanagihara D, Iino M, Watanabe M, Kano M (2005) Maintenance of presynaptic function by AMPA receptor-mediated excitatory postsynaptic activity in adult brain. *Proc Natl Acad Sci USA* 102: 19180-19185

Kakizawa S, Yamasaki M, Watanabe M, Kano M (2000) Critical period for activity-dependent synapse elimination in developing cerebellum. *J Neurosci* 20: 4954-4961

Kanemaru K, Okubo Y, Hirose K, Iino M (2007) Regulation of neurite growth by spontaneous Ca^{2+} oscillations in astrocytes. *J Neurosci* 27: 8957-8966

Kano M, Garaschuk O, Verkhratsky A, Konnerth A (1995) Ryanodine receptor-mediated intracellular calcium release in rat cerebellar Purkinje neurones. *J Physiol* 487: 1-16

Kettlun C, Gonzalez A, Rios E, Fill M (2003) Unitary Ca^{2+} current through mammalian cardiac and amphibian skeletal muscle ryanodine receptor Channels under near-physiological ionic conditions. *The Journal of general physiology* 122: 407-417

Kluge I, Gutteck-Amsler U, Zollinger M, Do KQ (1997) S-nitrosoglutathione in rat cerebellum: identification and quantification by liquid chromatography-mass spectrometry. *J Neurochem* 69: 2599-2607

Leach MJ, Swan JH, Eisenthal D, Dopson M, Nobbs M (1993) BW619C89, a glutamate release inhibitor, protects against focal cerebral ischemic damage. *Stroke* 24: 1063-1067

Lev-Ram V, Makings LR, Keitz PF, Kao JP, Tsien RY (1995) Long-term depression in cerebellar Purkinje neurons results from coincidence of nitric oxide and depolarization-induced Ca^{2+} transients. *Neuron* 15: 407-415

Lev-Ram V, Mehta SB, Kleinfeld D, Tsien RY (2003) Reversing cerebellar long-term depression. *Proc Natl Acad Sci USA* 100: 15989-15993

Lev-Ram V, Wong ST, Storm DR, Tsien RY (2002) A new form of cerebellar long-term potentiation is postsynaptic and depends on nitric oxide but not cAMP. *Proc Natl Acad Sci USA* 99: 8389-8393

Li F, Hayashi T, Jin G, Deguchi K, Nagotani S, Nagano I, Shoji M, Chan PH, Abe K (2005) The protective effect of dantrolene on ischemic neuronal cell death is associated with reduced expression of endoplasmic reticulum stress markers. *Brain Res* 1048: 59-68

Malinski T, Bailey F, Zhang ZG, Chopp M (1993) Nitric oxide measured by a porphyrinic microsensor in rat brain after transient middle cerebral artery occlusion. *J Cereb Blood Flow Metab* 13: 355-358

Moore CP, Zhang JZ, Hamilton SL (1999) A role for cysteine 3635 of RYR1 in redox modulation and calmodulin binding. *J Biol Chem* 274: 36831-36834

Mori F, Fukaya M, Abe H, Wakabayashi K, Watanabe M (2000) Developmental changes in expression of the three ryanodine receptor mRNAs in the mouse brain. *Neurosci Lett* 285: 57-60

Nakai J, Imagawa T, Hakamata Y, Shigekawa M, Takeshima H, Numa S (1990) Primary structure and functional expression from cDNA of the cardiac ryanodine receptor/calcium release channel. *FEBS Lett* 271: 169-177

Namiki S, Kakizawa S, Hirose K, Iino M (2005) NO signalling decodes frequency of neuronal activity and generates synapse-specific plasticity in mouse cerebellum. *J Physiol* 566: 849-863

Pacher P, Beckman JS, Liaudet L (2007) Nitric oxide and peroxynitrite in health and disease. *Physiol Rev* 87: 315-424

Peterson BZ, DeMaria CD, Adelman JP, Yue DT (1999) Calmodulin is the Ca^{2+} sensor for Ca^{2+}-dependent inactivation of L-type calcium channels. *Neuron* 22: 549-558

Sacchetti B, Scelfo B, Tempia F, Strata P (2004) Long-term synaptic changes induced in the cerebellar cortex by fear conditioning. *Neuron* 42: 973-982

Sawada K, Hosoi E, Bando M, Sakata-Haga H, Lee NS, Jeong YG, Fukui Y (2008) Differential alterations in expressions of ryanodine receptor subtypes in cerebellar cortical neurons of an ataxic mutant, rolling mouse Nagoya. *Neuroscience* 152: 609-617

Sham JS (1997) Ca^{2+} release-induced inactivation of Ca^{2+} current in rat ventricular myocytes: evidence for local Ca^{2+} signalling. *J Physiol* 500: 285-295

Sun J, Xin C, Eu JP, Stamler JS, Meissner G (2001) Cysteine-3635 is responsible for skeletal muscle ryanodine receptor modulation by NO. *Proc Natl Acad Sci USA* 98: 11158-11162

Sun J, Yamaguchi N, Xu L, Eu JP, Stamler JS, Meissner G (2008) Regulation of the cardiac muscle ryanodine receptor by O_2 tension and *S*-nitrosoglutathione. *Biochemistry* 47: 13985-13990

Takechi H, Eilers J, Konnerth A (1998) A new class of synaptic response involving calcium release in dendritic spines. *Nature* 396: 757-760

Takeshima H, Iino M, Takekura H, Nishi M, Kuno J, Minowa O, Takano H, Noda T, Yamazawa T, Ikemoto T, Nishiyama N, Shimuta M, Sugitani Y, Saito I, Saito H, Endo M, Sakurai T (1994) Excitation-contraction uncoupling and muscular degeneration in mice lacking functional skeletal muscle ryanodine-receptor gene. *Nature* 369: 556-559

Takeshima H, Ikemoto T, Nishi M, Nishiyama N, Shimuta M, Sugitani Y, Kuno J, Saito I, Saito H, Endo M, Iino M, Noda T, Yamazawa T, Sakurai T (1996) Generation and characterization of mutant mice lacking ryanodine receptor type 3. *J Biol Chem* 271: 19649-19652

Takeshima H, Nishimura S, Matsumoto T, Ishida H, Kangawa K, Minamino N, Matsuo H, Ueda M, Hanaoka M, Hirose T, Numa S (1989) Primary structure and expression from complementary DNA of skeletal muscle ryanodine receptor. *Nature* 339: 439-445

Wojcikiewicz RJ (1995) Type I, II, and III inositol 1,4,5-trisphosphate receptors are unequally susceptible to down-regulation and are expressed in markedly different proportions in different cell types. *J Biol Chem* 270: 11678-11683

Zhao F, Li P, Chen SR, Louis CF, Fruen BR (2001) Dantrolene inhibition of ryanodine receptor Ca^{2+} release channels. Molecular mechanism and isoform selectivity. *J Biol Chem* 276: 13810-13816

Zühlke RD, Pitt GS, Deisseroth K, Tsien RW, Reuter H (1999) Calmodulin supports both inactivation and facilitation of L-type calcium channels. *Nature* 399: 159-162

Figure legends

Figure 1 NO induces intracellular Ca^{2+} release via RyR1 in cerebellar Purkinje cells. (**A**) Confocal Ca^{2+} imaging of Purkinje cell dendrites (left) and pseudocolor Ca^{2+} imaging of cells (right) 120 s following NOC7 (300 μM) treatment. (**B**) NOC7-induced Ca^{2+} increase with or without thapsigargin (2 μM). (**C**) NOC7-induced Ca^{2+} increase at 36°C with or without dantrolene (30 μM). (**D**) Effect of various perturbations (i.e. removal of extracellular Ca^{2+} with 0.5 mM EGTA (0Ca), 2 μM thapsigargin (TG), 4 mg ml^{-1} heparin applied through a patch pipette (Hep), and 30 μM dantrolene (Dan)) on the peak magnitude of the NO-induced Ca^{2+} response. (**E**) Confocal Ca^{2+} imaging in the soma of neonatal Purkinje cells 120 s after NOC7 (300 μM) treatment in control and *Ryr1*$^{-/-}$ mice. (**F**) NOC7-induced Ca^{2+} increase in Purkinje cells treated with or without thapsigargin (2 μM) and in *Ryr1*$^{-/-}$ Purkinje cells. (G) Summary of the effect of perturbations on the magnitude of NO-induced Ca^{2+} increase. In all graphs, error bars indicate s.e.m. (n = 5–11). *P < 0.01, **P < 0.001, *t*-test compared with control.

Figure 2 NO-induced Ca^{2+} release in HEK293 cells expressing RyR1. (**A**) Effect of various perturbations [i.e. without tetracycline induction, control, removal of extracellular Ca^{2+} with 1 mM EGTA (0Ca), 2 μM thapsigargin (TG), 1 μM ODQ, control at 35°C, and 30 μM dantrolene] on the peak magnitude of NOC7 (300 μM)-induced Ca^{2+} increase; n = 50–145. (**B**) RyR subtype dependence of the NO-induced Ca^{2+} response. Please refer to

Supplementary Figure S2G for more information. (**C** and **D**) Ca^{2+} response to NOC7 and caffeine in HEK293 cells expressing RyR1 (left) or C3635A-RyR1 (right); *n* = 121–245. (**E**) Time-course of NOC7 (1 mM)-induced *S*-nitrosylation of wild-type and C3635A-RyR1 cells, as determined by the biotin switch method. (F) Summary of the time-course of *S*-nitrosylation; *n* = 3–4. In all graphs, error bars indicate s.e.m. *P < 0.02, **P < 0.001, *t*-test compared with control.

Figure 3 Nerve activity induces NICR in Purkinje cells. (**A**) Confocal Ca^{2+} imaging of Purkinje cell dendrites (left) and pseudocolor Ca^{2+} imaging of cells (right) 60 s after BS (5 pulses at 50 Hz repeated 60 times every 1 s). (**B**) Spatial distribution of BS-induced Ca^{2+} release; *n* = 5. (**C**) BS-induced Ca^{2+} increase in wild-type and *Nos1*$^{-/-}$ mice with or without thapsigargin (2 μM); *n* = 5–6. (**D**) BS-induced Ca^{2+} increase in wild-type mice with or without dantrolene (30 μM) at 36°C; *n* = 5–6. (**E**) Effect of various perturbations on the magnitude of BS-induced Ca^{2+} increase. Control, thapsigargin, heparin (4 mg ml^{-1}) applied through a patch pipette, ODQ (1 μM), cocktail of glutamate receptor antagonists (αGluR: 20 μM NBQX and 100 μM CPCCOEt), L-NAME (100 μM), *Nos1*$^{-/-}$, control at 36°C, and dantrolene, *n* = 5–7. In all graphs, error bars indicate s.e.m. *P < 0.01, **P < 0.001, *t*-test compared with control.

Figure 4 Involvement of NICR in synaptic plasticity. (**A**) Long-term potentiation (LTP) of excitatory postsynaptic currents (EPSCs) at the PF-PC synapse in wild-type and *Nos1*$^{-/-}$

mice; $n = 5$. (**B**) Dantrolene (30 μM) blocked PF-LTP at 36°C; $n = 5$–6. (**C**) Effect of various perturbations on the magnitude of LTP (normalized EPSC averaged between 21 min and 30 min after BS): control, thapsigargin (2 μM), heparin (4 mg ml^{-1}) applied through a patch pipette, CPCCOEt (100 μM, αmGluR), BAPTA (30 mM) applied through a patch pipette, control at 36°C, dantrolene (30 μM), and *Nos1*$^{-/-}$; $n = 4$–6. **P < 0.001, *t*-test compared with control.

Figure 5 Possible involvement of NICR in ischemic brain damage. (**A**) Representative triphenyltetrazolium chloride (TTC)-stained brain slices 24 h after transient MCAO. (**B**) Infarct volume 24 h after transient MCAO determined using the Leach correction; $n = 6$ for each condition. A two-way ANOVA revealed a significant interaction (P = 0.026), and subsequent analyses with Tukey's multiple comparison test indicated that *Nos1*$^{+/+}$ mice treated with dantrolene had a significantly smaller infarct volume compared with *Nos1*$^{-/-}$ mice. Data are the mean ± s.e.m.

Figure 6 Involvement of NICR in NO-induced neuronal cell death. (**A**) NOC12 (500 μM)-induced intracellular Ca^{2+} increase in cultured cerebral neurons of *Ryr1*$^{+/+}$ (left, $n = 30$ cells) or *Ryr1*$^{-/-}$ (right, $n = 28$ cells) mice. Ca^{2+} measurements were made in the absence of extracellular Ca^{2+}. (**B**) NOC12-induced Ca^{2+} release is blocked by dantrolene (10 μM) at 35°C. Control, $n = 22$ cells; dantrolene, $n = 21$ cells. (**C**) Neuronal cell death assayed 16 h after treatment with 500 μM NOC12 without or with 10 μM dantrolene in cultured cerebral

neurons of *Ryr1*$^{+/+}$ (left) or *Ryr1*$^{-/-}$ (right) mice. (**D**) The extent of cell death was expressed as a ratio of the number of propidium iodide-positive cells to that of Hoechst-positive cells. Numbers in parentheses (15–22) indicate the number of determinations in each condition using different cultures. In each determination >120 cells were analyzed. Data are the mean ± s.e.m. Statistical significance was determined via an ANOVA followed by a Tukey *post-hoc* test. ***P < 0.0001.

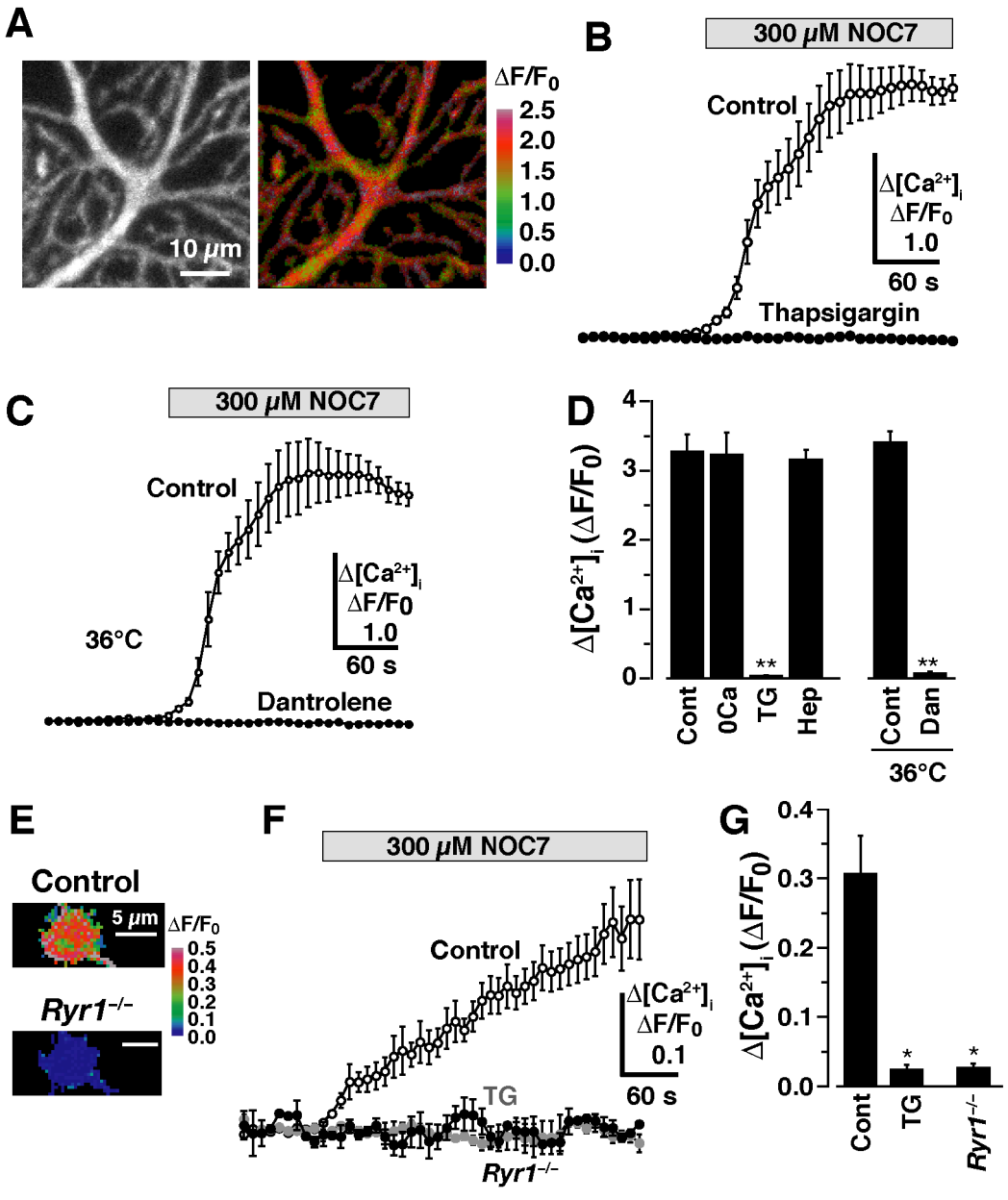
A
10 μm
ΔF/F0
2.5
2.0
1.5
1.0
0.5
0.0
B
300 μM NOC7
Control
Δ[Ca2+]i
ΔF/F0
1.0
60 s
Thapsigargin
C
300 μM NOC7
Control
36°C
Δ[Ca2+]i
ΔF/F0
1.0
60 s
Dantrolene
D
Δ[Ca2+]i (ΔF/F0)
4
3
2
1
0
**
**
Cont
0Ca
TG
Hep
Cont
Dan
36°C
E
Control
5 μm
ΔF/F0
0.5
0.4
0.3
0.2
0.1
0.0
Ryr1−/−
F
300 μM NOC7
Control
Δ[Ca2+]i
ΔF/F0
0.1
60 s
TG
Ryr1−/−
G
Δ[Ca2+]i (ΔF/F0)
0.4
0.3
0.2
0.1
0.0
*
*
Cont
TG
Ryr1−/−

Figure 1

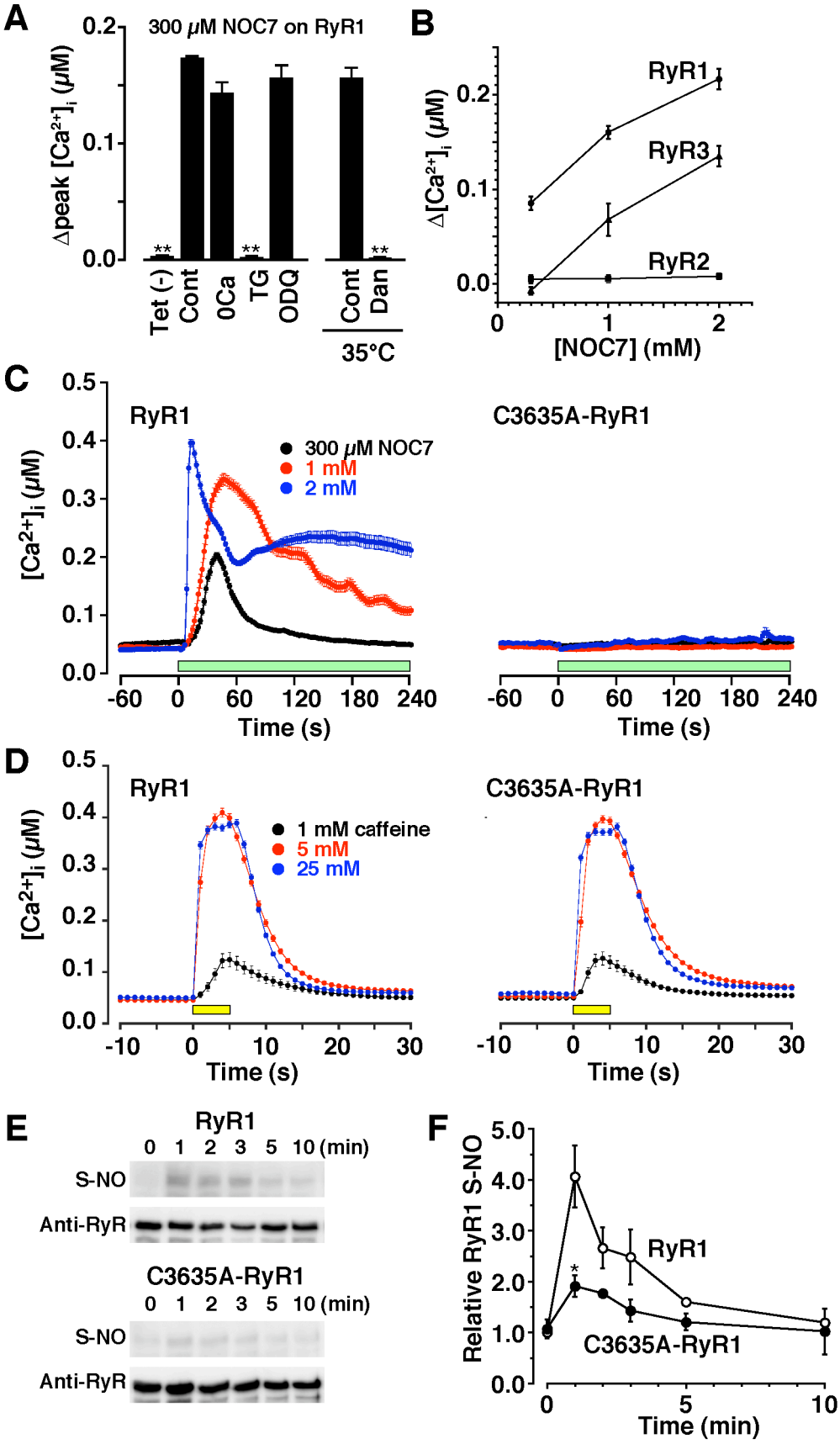
A
300 μM NOC7 on RyR1
Δpeak [Ca2+]i (μM)
0.2
0.1
0.0
**
**
**
Tet (-)
Cont
0Ca
TG
ODQ
Cont
Dan
35°C
B
RyR1
RyR3
RyR2
Δ[Ca2+]i (μM)
0.2
0.1
0.0
0
1
2
[NOC7] (mM)
C
RyR1
C3635A-RyR1
300 μM NOC7
1 mM
2 mM
[Ca2+]i (μM)
0.5
0.4
0.3
0.2
0.1
0.0
-60
0
60
120
180
240
Time (s)
D
RyR1
C3635A-RyR1
1 mM caffeine
5 mM
25 mM
[Ca2+]i (μM)
0.5
0.4
0.3
0.2
0.1
0.0
-10
0
10
20
30
Time (s)
E
RyR1
0 1 2 3 5 10 (min)
S-NO
Anti-RyR
C3635A-RyR1
0 1 2 3 5 10 (min)
S-NO
Anti-RyR
F
Relative RyR1 S-NO
5.0
4.0
3.0
2.0
1.0
0.0
RyR1
*
C3635A-RyR1
0
5
10
Time (min)

Figure 2

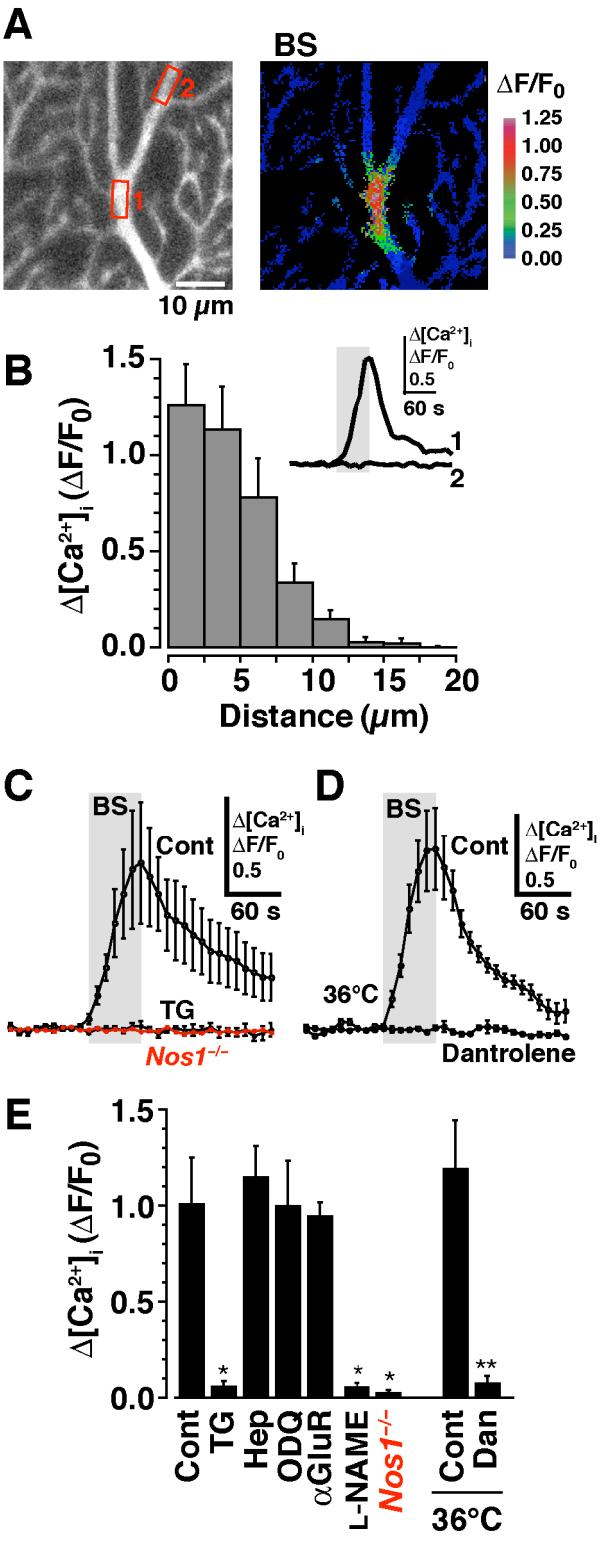
A
BS
ΔF/F0
1.25
1.00
0.75
0.50
0.25
0.00
2
1
10 μm
B
Δ[Ca2+]i (ΔF/F0)
1.5
1.0
0.5
0.0
0
5
10
15
20
Distance (μm)
Δ[Ca2+]i
ΔF/F0
0.5
60 s
1
2
C
BS
Cont
Δ[Ca2+]i
ΔF/F0
0.5
60 s
TG
Nos1−/−
D
BS
Cont
Δ[Ca2+]i
ΔF/F0
0.5
60 s
36°C
Dantrolene
E
Δ[Ca2+]i (ΔF/F0)
1.5
1.0
0.5
0.0
*
*
*
**
Cont
TG
Hep
ODQ
αGluR
L-NAME
Nos1−/−
Cont
Dan
36°C

Figure 3

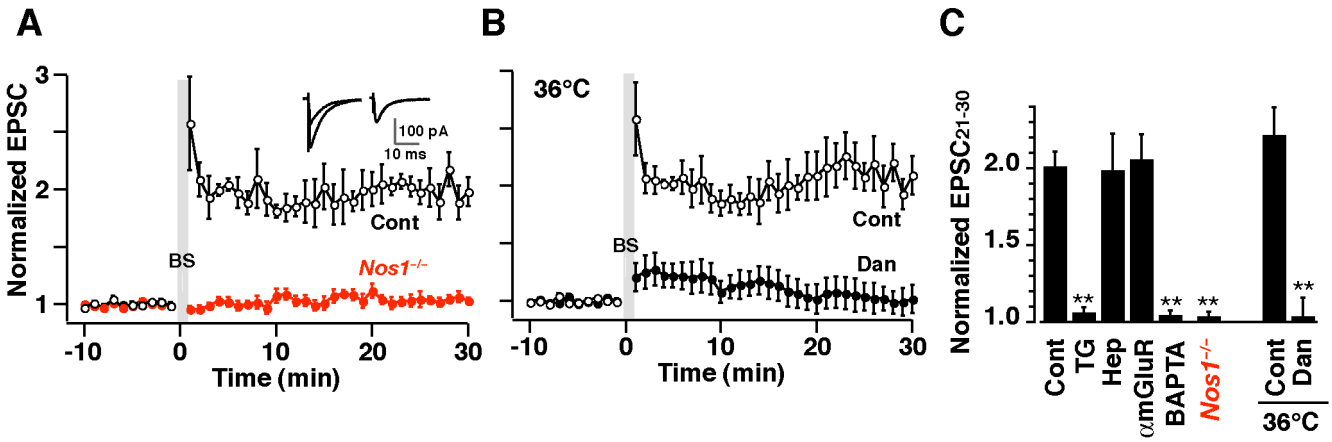
A
B
C
Normalized EPSC
3
2
1
100 pA
10 ms
Cont
BS
Nos1-/-
-10
0
10
20
30
Time (min)
36°C
Cont
BS
Dan
Normalized EPSC21-30
2.0
1.5
1.0
**
Cont
TG
Hep
αmGluR
BAPTA
Nos1-/-
Cont
Dan
36°C

Figure 4

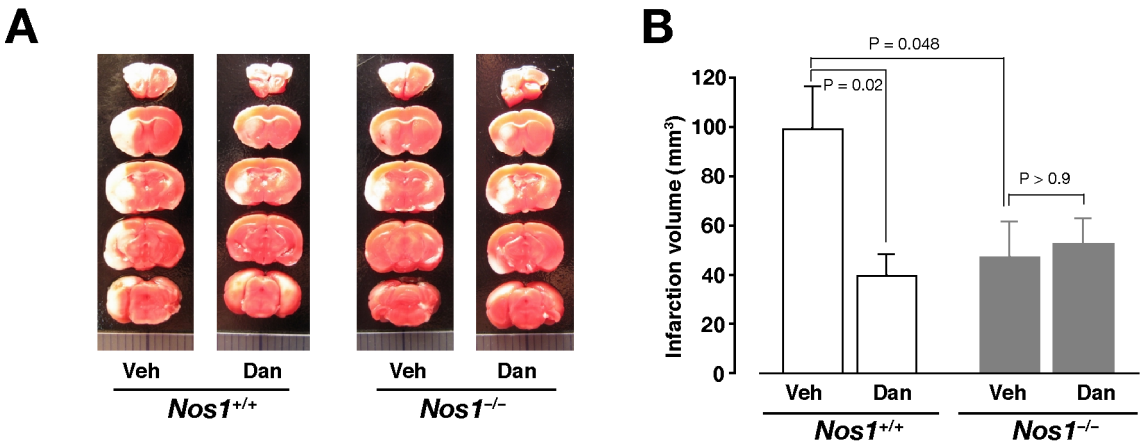
A
Veh
Dan
Veh
Dan
Nos1+/+
Nos1−/−
B
P = 0.048
P = 0.02
P > 0.9
Infarction volume (mm3)
120
100
80
60
40
20
0
Veh
Dan
Veh
Dan
Nos1+/+
Nos1−/−

Figure 5

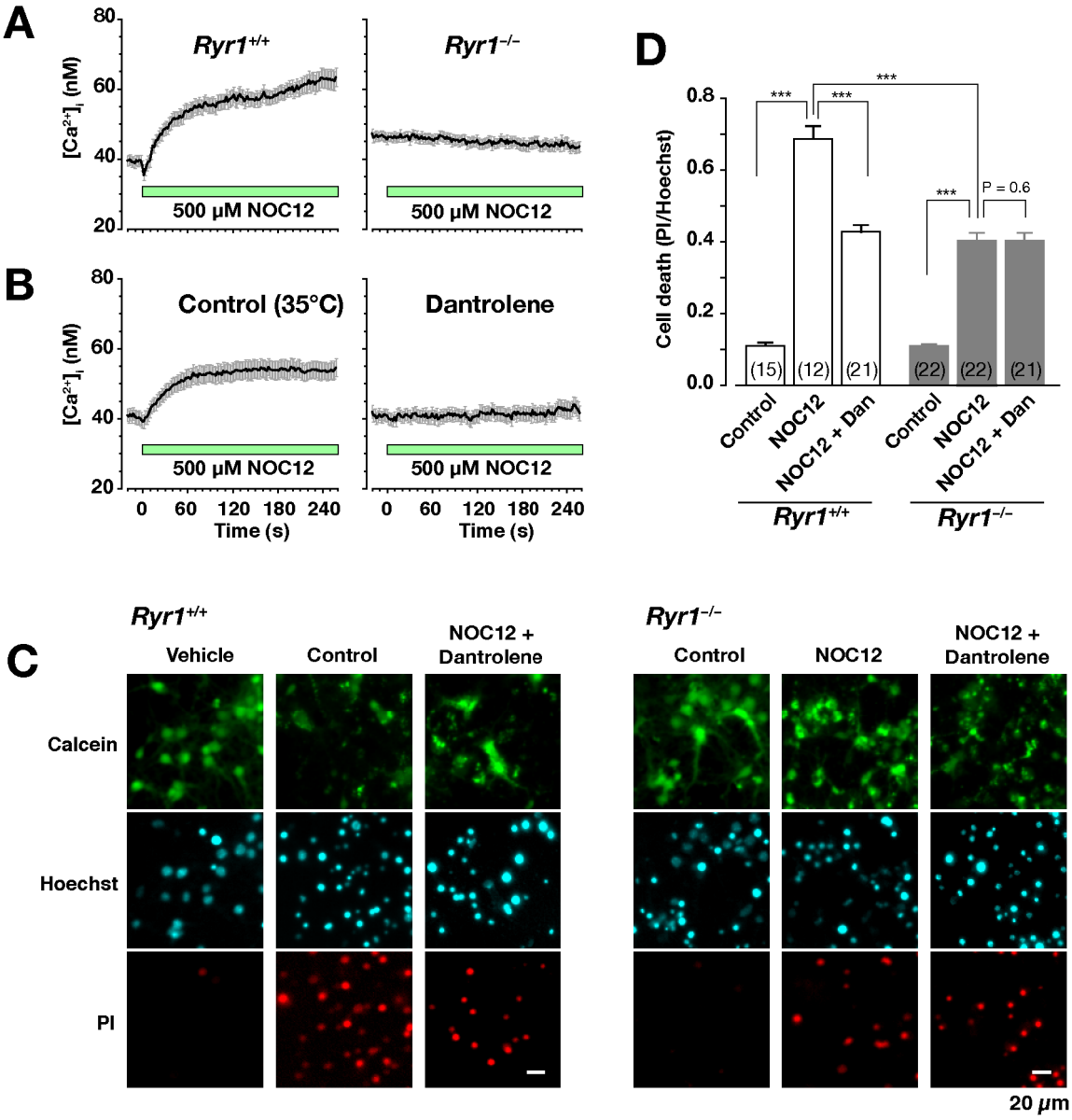
A
Ryr1+/+
Ryr1−/−
[Ca2+]i (nM)
80
60
40
20
500 µM NOC12
500 µM NOC12
B
Control (35°C)
Dantrolene
[Ca2+]i (nM)
500 µM NOC12
500 µM NOC12
0 60 120 180 240
Time (s)
0 60 120 180 240
Time (s)
D
Cell death (PI/Hoechst)
0.8
0.6
0.4
0.2
0.0
***
***
***
P = 0.6
(15) (12) (21) (22) (22) (21)
Control
NOC12
NOC12 + Dan
Control
NOC12
NOC12 + Dan
Ryr1+/+
Ryr1−/−
C
Ryr1+/+
Vehicle
Control
NOC12 + Dantrolene
Ryr1−/−
Control
NOC12
NOC12 + Dantrolene
Calcein
Hoechst
PI
20 µm

Figure 6